Simulating the Effect of Fracture Connectivity on Repository Performance with GDSA Framework – 18589

S. David Sevougian*, Emily R. Stein*, Glenn E. Hammond*, Paul E. Mariner*, Jennifer M. Frederick*, and Eduardo Basurto*

*Sandia National Laboratories, PO Box 5800, MS 0747, Albuquerque, NM 87185, sdsevou@sandia.gov

ABSTRACT

This work examines the possible migration of radionuclides from a deep geologic nuclear waste repository sited in fractured crystalline host rock. The key safety concern is the potential effect on waste isolation of the inter-connectivity of the fracture network, which is primarily established by the temporal evolution of the temperature and stress fields at the time of original rock deposition. Two end members are considered in these simulations, one with a high degree of connectivity to the biosphere, such that advective transport through the fracture and fault network controls radionuclide migration, and the other with a low degree of connectivity, such that slow diffusive transport through the crystalline rock matrix is the controlling process for migration to the biosphere. Both end members have several areally extensive, high-transmissivity deformation zones, whose distance to the repository is an important factor for waste isolation capability. Uncertainties in fracture properties (transmissivity, orientation, radius) and fracture distribution also give rise to uncertainty in waste isolation capability (i.e., the overall connectivity of the repository with the surface biosphere). These types of natural system uncertainties are generally present in any geologic site-characterization program and thus represent an important factor in assessing repository performance in hard rock environments.

The waste considered in these simulations are spent fuel rod assemblies from the U.S. commercial nuclear reactor fleet. Thermal output of the waste must be considered in the simulations and can influence the rate and timing of waste package failure, waste form degradation, and fluid flux due to thermal expansion around the repository horizon. To achieve a high-fidelity representation of radionuclide transport in fractures and rock matrix, combined with thermal energy transport and fluid flow in fractures and matrix, the mathematical model is solved numerically in a parallel high-performance computing (HPC) environment on a finite volume unstructured grid consisting of approximately 5 million cells, using *Geologic Disposal Safety Assessment* (*GDSA*) *Framework* (https://pa.sandia.gov), an open-source performance assessment tool for deep underground disposal of nuclear waste. *GDSA Framework* uses PFLOTRAN to solve the balance equations on a three-dimensional grid with heterogeneous properties, using multiple processors in a parallel configuration based on domain decomposition.

The fracture networks in these simulations are originally generated as discrete fracture networks (DFNs), which are sets of two-dimensional planes distributed in a three-dimensional domain. The method used in *GDSA Framework* maps the stochastically generated DFN to an equivalent continuous porous medium (ECPM) domain that allows for the simulation of coupled heat flow, fluid flow, and radionuclide transport, including heat conduction through the matrix of the fractured rock, which is a process not easily modeled in a DFN representation. Computational efficiency is also greatly enhanced using the ECPM method, allowing for a realistic representation and analysis of uncertainties in a multi-realization performance assessment of a deep geologic repository.

The effect of fracture connectivity on the waste isolation safety function, as brought to light by these *GDSA Framework* simulations, points to the importance of including a realistic representation of uncertainties in fracture properties and distribution (effectively, uncertainty in spatial heterogeneity) in repository safety assessment simulations.

INTRODUCTION

Development of an enhanced performance assessment (PA) capability for geologic disposal of SNF and HLW has been ongoing for several years in the U.S. repository program [1, 2]. This enhanced PA capability, i.e., the *Geologic Disposal Safety Assessment (GDSA) Framework* (https://pa.sandia.gov), is based on open-source software architecture and configured to run in a massively parallel, high-performance computing (HPC) environment. It consists of two main components, the open-source Dakota uncertainty sampling and analysis software [3] and the PFLOTRAN multi-phase flow and reactive transport simulator [4, 5]. All geologic media (e.g., crystalline, argillite, salt) are currently under consideration; however, the simulations reported herein are for a mined repository approximately one-half kilometer below the ground surface in sparsely fractured crystalline host rock, such as granite or metagranite. Regionally, the topographic slope is less than 1 degree, and the water table is unconfined, a combination which would provide little driving force for deep fluid flow. The reference repository site has a stable cratonic terrain with low probabilities of seismicity, igneous activity, and human intrusion. The latter probability is reduced by avoiding regions with known geologic resources such as extensive fresh water aquifers, ore deposits, fossil fuels, or high geothermal heat flux (which offers the potential for geothermal development). This concept is consistent with international concepts of disposal in crystalline rock [6-9].

The current crystalline reference case repository [10] comprises a series of mined parallel disposal drifts (tunnels) connected by access halls. Repository access would be via vertical shafts and/or a ramp. Within the disposal drifts, SNF waste packages are centered in a cylindrical buffer consisting of compacted bentonite pellets and/or bricks. The bentonite buffer serves as an impermeable barrier to bulk movement of pore water, effectively isolating the waste container (and its radionuclide inventory) from connection with possible fractures in the host rock and the disturbed rock zone (DRZ) surrounding the drift excavation. If the buffer successfully fulfills its isolation safety function, the only mode of radionuclide transport from a breached waste package to the surrounding host rock is via the very slow process of molecular diffusion. This is the case for an undisturbed (nominal-evolution) scenario. However, this alone does not insure long-term isolation from the biosphere, since after radionuclides diffuse across the buffer barrier they enter the host rock wherein faster advective transport can occur if the fracture network is inter-connected. The question investigated herein is how uncertainties in fracture inter-connectivity affect predictions of waste isolation, i.e., predictions of the rate of radionuclide transport through the crystalline host rock. Although full uncertainty distributions in underlying fracture properties (orientation, size, and transmissivity) should be included in probabilistic PA representations, these distributions will generally result in a binary condition of fracture connectivity—either the repository is connected to the surface via a set of intersecting fractures and fault zones or it is not. The effect of this binary result is examined herein. For the condition of fracture/fault inter-connectivity to the surface, the assumed horizontal regional hydraulic gradient results in fast advective radionuclide transport to the ground surface, whereas for the condition of no fracture pathway to the surface, slower diffusive radionuclide transport improves the waste isolation capability of the repository system.

CRYSTALLINE HOST-ROCK REFERENCE CASE

The representation of fractured crystalline rock in the generic repository is based primarily on the well-characterized, sparsely fractured metagranite at Forsmark, Sweden [11, 12]. The Forsmark site is in the Fennoscandian Shield and consists of crystalline bedrock (primarily granite with lesser amounts of granodiorite, tonalite, and amphibolite) that formed between 1.89 and 1.85 Ga (1 Ga = 1 billion years), experienced ductile deformation and metamorphism, and cooled to the limit of brittle deformation between 1.8 and 1.7 Ga [13]. Crystalline basement with similar history exists within the United States [14], and can be reasonably expected to have similar hydraulic properties. Conceptually, the crystalline host rock is comprised of two media: fractures and matrix. Numerically it is simulated in *GDSA Framework* with two

types of grid cells: those containing a fracture or fractures and those without fractures (the matrix). Hydraulic parameters (permeability and porosity) describing fracture grid cells are derived from fracture parameters developed for the Forsmark metagranite [11, 12, 15]. Hydraulic parameters describing matrix cells are derived from measurements made in tunnel walls of underground research laboratories (URLs) in crystalline rock at the Grimsel Test Site, Switzerland [16, 17], Lac du Bonnet batholith, Canada [18], and the Korean Underground Research Tunnel [19]. All other parameters are identical in fracture and matrix cells.

It is assumed that a deep geologic repository would hold 70,000 MTHM of CSNF, which is the maximum allowed by the Nuclear Waste Policy Act of 1983 and about half of the total CSNF inventory predicted by 2055 in a "no replacement scenario," [20] i.e., no replacement of current nuclear reactors and no new builds, with 60-year lifetimes assumed for all current reactors. This inventory could be accommodated in 168 horizontal disposal drifts, each 805 m in length, with drift centers separated by 20 m, and waste packages emplaced lengthwise within the drifts with a spacing of 10 m center-to-center [15]. Repository access would be via vertical shafts and/or a ramp. Approximately one quarter of the 70,000 MTHM inventory is included in 42 disposal drifts in PA simulations discussed below.

The CSNF waste package is assumed to consist of a stainless-steel canister containing 12 PWR CSNF assemblies (5.22 MTHM) and a stainless steel overpack, 5 meters in length and 1.29 m in diameter. Due to gridding limitations, the size of simulated waste packages is $1.67 \times 1.67 \times 5$ m^3, and is slightly larger in volume than 12-PWR waste packages are expected to be. Waste package porosity is set equal to the fraction of void space within a waste package, which is 50% [21]. Permeability is set several orders of magnitude higher than that of the surrounding materials, so that flow through waste packages is uninhibited. The waste package is given the thermal properties of stainless steel [22]. The granite reference case described here represents waste package performance via an Arhennius-type relationship for general corrosion, which calculates the remaining waste package thickness at any time [23]. Each waste package is modeled as a transient heat source. The energy (watts per waste package) entering the model domain is updated each time step from values in a lookup table. The initial value (3084 W/waste package) is that for PWR CSNF 100 yr OoR. Between times specified in the lookup table, the energy input is linearly interpolated. The waste package degradation model implemented in PFLOTRAN [10] calculates fractional canister thickness at each time step as a function of a base canister degradation rate, a canister material constant, and temperature. Waste package breach occurs when the fractional canister thickness reaches zero. A base canister degradation rate is assigned to each waste package from a truncated log-normal distribution with a mean of $10^{-4.5}$/yr, a standard deviation of 0.5 (log units) and an upper truncation of –3.5 (log units).

Waste packages are assumed to be elevated on plinths of compacted bentonite and emplacement drifts are buffered and filled with compacted bentonite pellets and/or bricks in one or two layers [15]. Access halls may be filled with a mixture of crushed rock and bentonite or another geologic material rich in clay minerals [7, 15], but the present simulations assume the access halls and drifts are both filled with a compacted bentonite buffer. Compacted bentonite has low permeability, high sorption capacity, and may be engineered to achieve desirable thermal properties; for instance, quartz sand or graphite can be added to increase its thermal conductivity [24, 25, 26]. The current set of simulations employs a single layer buffer with material properties appropriate for a compacted mixture of 70% bentonite and 30% quartz sand. The buffer is assigned a porosity of 0.35 [27], a permeability of 10^{-20} m^2 [27], and a water-saturated thermal conductivity of 1.5 W/m/K [26]. Fig. 1 is a graphical depiction of repository layout in the *GDSA Framework* simulations.

For simplicity, PA simulations assume the inventory consists entirely of pressurized water reactor (PWR) CSNF assemblies, each containing 0.435 MTHM. Radionuclide inventories and decay heat as a function of time assume an initial enrichment of 4.73 weight-% ^{235}U, 60 GWd/MTHM burn-up, and 100-yr out-of-reactor (OoR) storage prior to deep geologic disposal [20]. Because the average burn-up of CSNF under

the no-replacement scenario is predicted to be only 54 GWd/MTHM [20], the assumption of 60 GWd/MTHM results in a conservatively high heat load.

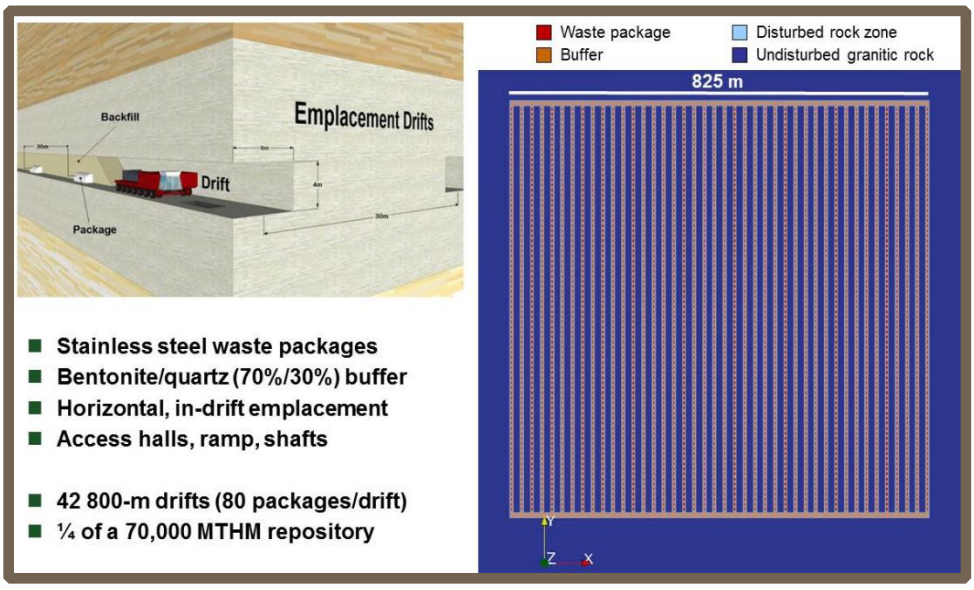

Fig. 1. Engineered barrier system and repository layout for the simulated generic repository in crystalline host rock.

PFLOTRAN calculates decay and ingrowth of the radionuclide inventory in each waste package region. From the time of waste package breach, the uranium oxide (UO_2) waste form releases radionuclides in two fractions: instant-release and slow-release. The instant-release fraction is due to the accumulation of fission products in waste form void spaces and occurs right at waste package breach. The crystalline reference case assumes a non-zero instant-release fraction for ^{135}Cs, ^{129}I, ^{99}Tc, and ^{36}Cl (0.1, 0.1, 0.07, and 0.05, respectively [28]), and zero for all other radionuclides. The slow-release fraction is due to fuel matrix (UO_2) dissolution, modeled here using a fractional dissolution rate of 10^{-7}/yr starting from the time of first waste package breach. This rate is the mode of a log-triangular distribution appropriate for fuel 3,000 to 10,000 years OoR under strongly reducing conditions [29].

Fig. 2 shows the heat of decay versus time for 60 GWd/MTHM spent UO_2 fuel, as well as calculated time histories of waste form degradation and waste package failure rate.

The DRZ, the portion of the host rock adjacent to the engineered barrier, will have elevated permeability due to changes in stress induced by mining. *In-situ* DRZ permeability has been measured in URLs in crystalline rock in Korea [19] and Canada [18]. In the Korean URL, gas permeability was as high as 10^{-17} m^2 at distances up to two meters from the tunnel wall; beyond that distance it was approximately 10^{-20} m^2 (liquid permeabilities are less than low-pressure gas permeabilities) [19]. In the Lac du Bonnet URL in Canada, liquid permeability was between 10^{-16} and 10^{-19} m^2 out to 0.3 to 0.5 m from the tunnel wall, beyond which it was between 10^{-22} and 10^{-20} m^2 [18]. PA simulations assume a 1.67 m thick DRZ on all sides of emplacement drifts and access halls. DRZ porosity is assumed to be 0.01, twice that of the undisturbed matrix; the effective diffusion coefficient is assumed to be 10^{-11} m^2, 10 times higher than undisturbed host rock; and DRZ permeability is assumed to be 10^{-16} m^2, the highest value measured in the Lac du Bonnet URL [18].

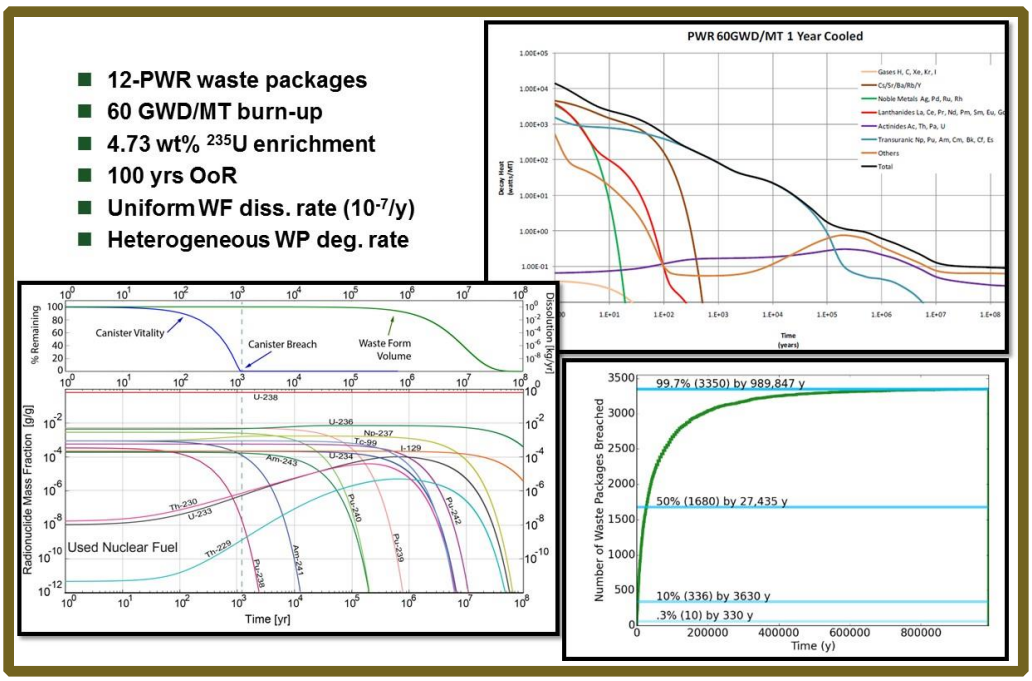

Fig. 2. Inventory, decay heat, waste form degradation rate, and waste package failure rate for the simulated generic repository in crystalline host rock. [Note: "Canister vitality" is defined as the remaining fraction of waste package thickness, i.e., the fraction not as yet degraded by general corrosion.]

Simulations use element solubility limits calculated by Mariner et al. [7] for a dilute Na-Ca-Cl brine at nearly neutral pH under reducing conditions. I, Cl, and Cs are assumed to be infinitely soluble. Isotope solubility is calculated assuming that isotope ratios are identical in the solid and aqueous phases [10]. Sorption is modeled using linear distribution coefficients (K_d values) [10]. I and Cl are assumed to be non-sorbing.

POST-CLOSURE PERFORMANCE ASSESSMENT SIMULATIONS

Conceptual and Numerical Model

Simulations assume a mined repository at 585 m depth in fractured crystalline rock, with saturated hydraulic conditions; overlain by a thin 15-meter layer of unconsolidated sedimentary overburden, comprised of glacial sediments with porosity (0.2) and permeability (10^{-15} m^2) appropriate for a silty glacial till [30]. Pressures and temperatures are initialized by applying zero liquid flux and an energy flux of 60 mW/m^2 to the base of the domain, while holding temperature (10°C) and pressure (approximately atmospheric) constant at the top of the domain. Pressure at the top of the domain decreases from west (left) to east (right) with a gradient of −13 Pa/m. Simulations include 18 radionuclides (^{241}Am, ^{243}Am, ^{238}Pu, ^{239}Pu, ^{240}Pu, ^{242}Pu, ^{237}Np, ^{233}U, ^{234}U, ^{236}U, ^{238}U, ^{229}Th, ^{230}Th, ^{226}Ra, ^{135}Cs, ^{129}I, ^{99}Tc, ^{36}Cl); initial concentrations of all radionuclides in all cells are 10^{-22} mol/L. Concentration of each radionuclide in fluid entering the model domain is 10^{-22} mol/L, while fluid exiting the model domain is allowed to advect ambient concentrations (no diffusive flux at boundaries). Material properties are summarized in TABLE 1.

The generic post-closure PA is currently focused on the undisturbed, nominal-evolution scenario (e.g., no human intrusion, seismicity, or glacial fluid influx), with slow corrosion of the waste package and diffusive releases through the buffer. Because the generic PA does not presently consider the biosphere, the performance metric is maximum radionuclide concentration in the sedimentary overburden, rather than

annual dose. PA simulations were implemented within the *Geologic Disposal Safety Assessment (GDSA) Framework* [10, 31]—https://pa.sandia.gov, which employs PFLOTRAN [4, 5] for numerically solving the energy, flow, and transport equations and Dakota for probabilistic sampling and analysis [3]. Parallelization in PFLOTRAN is achieved through domain decomposition using the Portable Extensible Toolkit for Scientific Computation (PETSc) [32]. PFLOTRAN is written in Fortran 2003/2008 and leverages state-of-the-art Fortran programming (i.e. Fortran classes, pointers to procedures, etc.) to support its object-oriented design. The Dakota toolkit is an analysis package for uncertainty quantification, sensitivity analysis, optimization, and calibration, for a parallel computing environment. The unstructured finite-volume mesh was gridded with Cubit [33].

TABLE 1. Material properties.

Material	Permeability, Log k m^2	Porosity, ϕ	Tortuosity, τ	Effective diffusivity, D_e[b] m^2/s	Thermal conductivity, λ W/m/K	Heat capacity, C_p J/kg/K	Grain density, ρ_g kg/m^3
Waste Package	−16	0.5	1	5×10^{-10}	16.7	466	5000
Buffer	−20	0.35	0.35	1.2×10^{-10}	1.5	830	2700
DRZ	−16	0.01	1	10^{-11}	2.5	830	2700
Matrix	−20	0.005	0.2	10^{-12}	2.5	830	2700
Fractures	[a]	[a]	[a]	10^{-12}	2.5	830	2700
Sediment	−15	0.2	0.2	4×10^{-11}	1.7	830	2700

[a] Calculated on a cell by cell basis for each fracture realization.
[b] $D_e = D_w\varphi\tau s$, where s is the liquid saturation, assumed here to be = 1, and D_w is the free water diffusion coefficient $= 1\times10^{-9} m^2/s$ [34].

Discrete fracture networks (DFNs), networks of two-dimensional planes distributed in a three-dimensional domain, are commonly used to simulate isothermal fluid flow and particle transport in fractures [35], but unless coupled to a continuum, are incapable of simulating heat conduction through the rock matrix, and therefore incapable of capturing the effects of thermally driven fluid fluxes or of coupling chemical processes to thermal processes. In the PA simulations presented here a stochastically generated DFN is mapped to an equivalent continuous porous medium (ECPM), which allows representation of porous and fractured media in the same domain, captures the behavior of radionuclide transport in fractured rock, and allows simulation of coupled heat and fluid flow including heat conduction through the matrix of the fractured rock.

Fracture locations, sizes, and properties in the PFLOTRAN simulation domain are first generated as discrete fracture networks (DFNs) using dfnWorks [36], and then mapped to an equivalent continuous porous medium (ECPM) with a Python script called mapDFN.py [10]. Parameter inputs to dfnWorks are statistical distributions describing fracture orientation and fracture radii, fracture density (fractures per km^3), parameters relating fracture transmissivity (m^2/s) to fracture radius, and the dimensions of the three-dimensional model domain.

dfnWorks distributes fractures randomly within the space of the model domain. The user can choose to keep only those fractures that belong to a cluster of at least two fractures or that belong to a cluster connecting at least two faces of the domain, since isolated fractures have no real impact on waste isolation. For each retained fracture, dfnWorks returns the coordinates of the fracture center, the unit vector defining the pole normal to the plane of the fracture, and the fracture radius, permeability, and aperture (which is calculated as a function of the fracture transmissivity according to the cubic law [37]). mapDFN takes as input the output from dfnWorks and parameters describing the desired ECPM model domain and discretization, including the origin and extent of the domain and the size (length) of the cubic grid cells. It

determines intersections of fractures with grid cells, and calculates grid cell permeability and porosity from fracture permeability and aperture.

Anisotropic grid cell permeability is calculated from intrinsic fracture transmissivity by summing the contributions of all the fractures intersecting the cell [38]. In the calculation of porosity for each ECPM fracture grid cell, a simplifying assumption is made that each fracture intersecting the cell does so parallel to a face of the cell. Then the porosity (ϕ) of the cell is equal to $\left(\sum b_f\right)/d$, where d is the length of the cell side, and b_f is the aperture of fracture f. This value is the fracture porosity, which is a very small fraction of the total porosity in a fractured crystalline rock. mapDFN assigns user-specified values for matrix (i.e., background) permeability and porosity to all cells in the domain not intersected by fractures.

Fig. 3 shows a comparison of bulk permeability obtained using ECPM and DFN representations of identical fracture networks. ECPM simulations ran in a fraction of the time required for DFN simulations (~5 and ~30 minutes to run to 100,000 yr, respectively) and simulation results compare well. Bulk permeability (calculated from Darcy's Law [30]) in ECPM model domains is about 70% of that in the DFN domains. False connectivity and increased path length are two known challenges in creating ECPM representations of DFNs [39]. However, false connections can be minimized with asymmetric representations of permeability [39] without refining the grid discretization. Path lengths (and therefore travel times) are longer in ECPMs because the ECPM converts a sloped fracture plane from dfnWorks into a series of stair steps. Fracture permeability in the ECPM can be corrected to account for the difference in path length [39]. Corrections to ECPM permeability that minimize false connections and path length discrepancies may be included in *GDSA Framework* in the future.

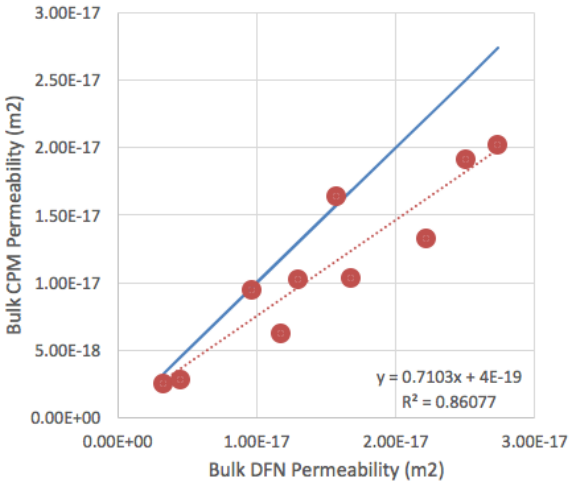

Fig. 3. Bulk permeability of ECPM versus DFN (from Stein et al. [38]).

Simulation Domain and Fracture Network Connectivity

As discussed by Mariner et al. [10], the representation of fractured crystalline rock in this analysis is based primarily on the well-characterized, sparsely fractured metagranite at Forsmark, Sweden [11, 12]. At Forsmark, large-scale mappable features of concentrated brittle and/or ductile deformation (termed "deformation zones") bound volumes of relatively undeformed rock. Each volume of relatively undeformed rock (termed a "fracture domain") is sparsely fractured, and the fractures within each can be described in terms of a number of "fracture sets," distinguished from each other on the basis of fracture orientation. At Forsmark six fracture domains are defined, each containing five fracture sets. As appropriate, three depth zones are defined (< 200 m below sea level (mbsl), 200 – 400 mbsl, and > 400 mbsl), in order to account for the decrease in fracture density and fracture transmissivity with depth. Each fracture set within a

particular fracture domain and depth zone is described using a 3-dimensional Fisher distribution to describe the orientation of fracture poles in space, a truncated power-law distribution for fracture radii, and a fracture density, P_{32}, which is defined as the surface area of fractures per volume of rock (m^2/m^3). For each depth zone within a fracture domain, a relationship is given between fracture radius and fracture transmissivity.

Relative to the Forsmark fracture characterization, several assumptions are made [10, Sec. 4.2.2.1] for the simulations and fracture connectivity study presented here. The most important of these is that only three fracture sets are simulated per depth zone, namely, those with the largest number of open and flowing fractures (NS, NE, and HZ; [11]), as shown in TABLE 2. [Note: The three "EW"-labeled fracture sets in TABLE 2 are based on the properties of Forsmark NE fracture sets but have been reoriented here to be parallel to the direction of flow. Also, only the 3 fracture sets associated with the top of the repository model domain (depth = 0 – 200 m in TABLE 2) were used to compare the bulk permeability of ECPM and DFN representations of fracture networks shown in Fig. 3.]

TABLE 2. Parameters used to generate discrete fracture networks using dfnWorks.

		Orientation: Fisher Distribution			Radius: Truncated Power Law			Spatial Density
Depth (m)	Fracture Set	Mean trend	Mean Plunge	κ	α	r_0 (m)	r_x (m)	(km^{-3})
0 – 200	**NS**	90°	0°	22	2.5	15	500	173
	EW	180°	0°	22	2.7	15	500	321
	HZ	360°	90°	10	2.4	15	500	1875
200 – 400	**NS**	90°	0°	22	2.5	15	500	337
	EW	180°	0°	22	2.7	15	500	347
	HZ	360°	90°	10	2.4	15	500	1091
> 400	**NS**	90°	0°	22	2.5	15	500	223
	EW	180°	0°	22	2.7	15	500	164
	HZ	360°	90°	10	2.4	15	500	487

The Fisher and power-law distributions in TABLE 2 are sampled randomly to generate 100 fracture maps, i.e., 100 stochastic realizations of fracture orientation, size, and permeability across the simulation domain. Each realization contains approximately 9,000 stochastically generated connected fractures. An example of one realization, i.e., a single stochastically generated fracture map, is shown in Fig. 4 (along with several deterministic features—high-permeability deformation zones—used in the PA simulations).

Fracture permeability (actually, transmissivity) for all fractures in the DFN network (e.g., all fractures in Fig. 4) is calculated as a function of fracture radius according to [11]:

$$\log(T_f) = \log(ar^b), \qquad \text{(Eq. 1)}$$

where T_f is fracture transmissivity (m^2/s), r is fracture radius (m), and a and b are constants with values of 1.6×10^{-9} and 0.8, respectively. As mentioned above, these transmissivities are then assigned to ECPM grid cells by summing the transmissivities of all fractures intersecting a grid cell, and then converting to fracture permeability (i.e., permeability of "fracture" ECPM grid cells) by dividing by the length of the cell side, d. The use of Eq. 1 for fractures at all depths in the model domain results in an overestimation of fracture transmissivity for fractures at depths greater than 200 m [10, Sec. 4.2.2.1].

The other key parameter for fracture inter-connectivity to the surface is the distance between the edge of the repository and the closest large-scale deformation zone. Fig. 5 shows the simulation domain and

repository region for fracture-map realization #3, indicating three fixed fault zones (gray) and two fixed sub-vertical deformation zones (red). These five features are at the same location in all 100 fracture maps. The nearest deterministic feature to the repository, i.e., the middle of the three vertical faults in Fig. 5, is the main controlling factor for inter-connectivity to the surface. The probability of fracture/fault connectivity to the surface has been computed as a function of the distance of this particular fault from the edge of the repository. This probability is calculated as the fraction of the 100 dfnWorks realizations that connect the repository to the sedimentary overburden via any continuous path through the deformation/fault zones and the fracture network (i.e., any path of connected ECPM "fracture" grid cells), and is plotted as a histogram (probability vs. distance) in Fig. 6. Five "observation points" in the sedimentary layer are also indicated in Fig. 5, which are used to examine radionuclide breakthrough to the surface (see next section).

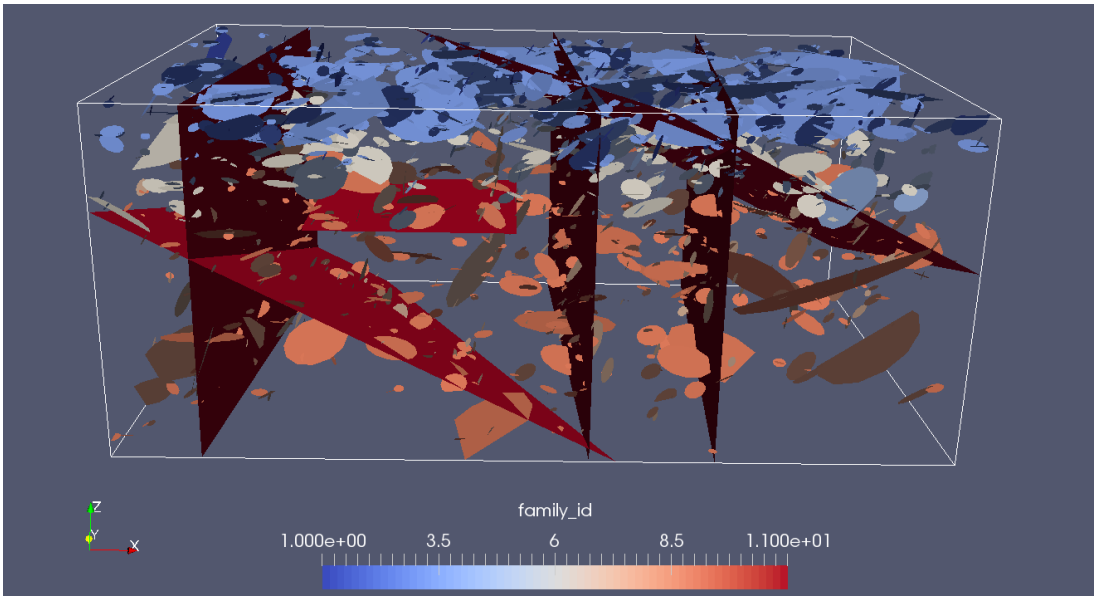

Fig. 4. A typical fracture-map realization, generated with 9 fracture sets described in TABLE 2.

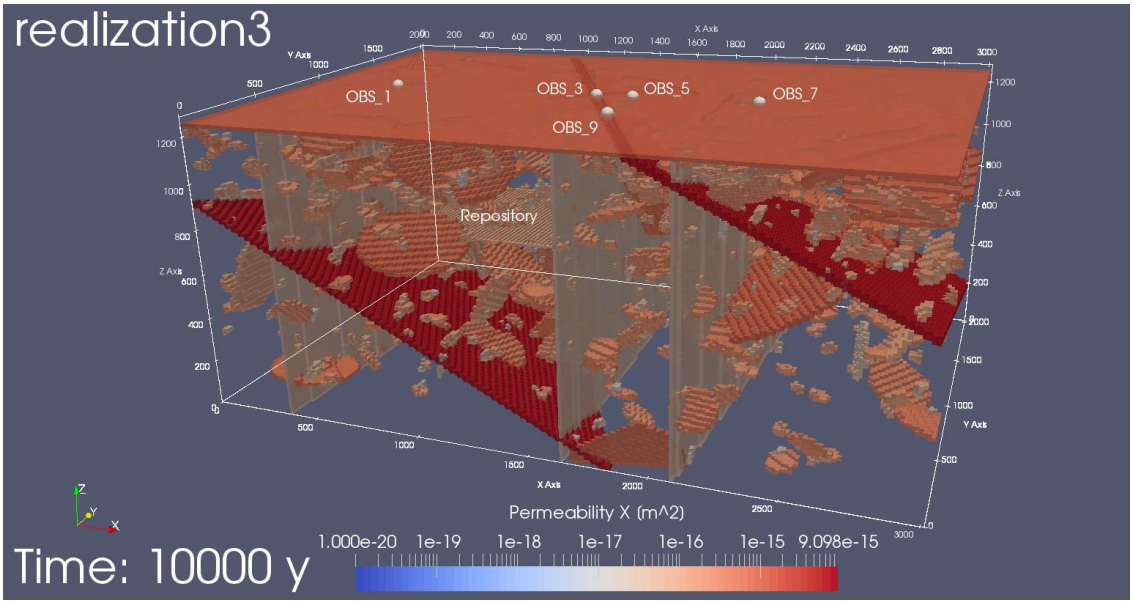

Fig. 5. PFLOTRAN simulation domain for the generic crystalline repository, showing a "connected" realization of the fracture network.

The simulation domain in Fig. 5 is 3015 m × 2025 m × 1260 m. The grid cells are mostly 15 meters on a side (in the far field), but in the repository region (around the waste packages) are as small as 1.67 meters on a side. The result is about 4.8 million grid cells, which requires about eight hours of wall-clock time on 512 cores, for each million-year simulation of repository performance.

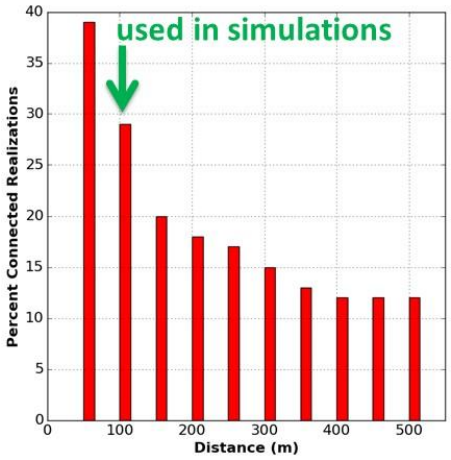

Fig. 6. Fraction ("probability") of the 100 fracture maps that connect the repository to the sedimentary overburden, as a function of the distance of the nearest vertical feature to the edge of the repository.

Simulation Results – Time Histories of ^{129}I Breakthrough at the Surface

^{129}I time histories at Observation Point #7, which is at the top of the vertical feature farthest downgradient from the simulated repository, are shown in Fig. 7. As indicated in Fig. 6, for the case of 100 meters distance between the nearest vertical fault and the repository edge, 29 of the fracture-map realizations had direct fracture/feature pathway connectivity to the surficial sediments, while 71 fracture maps did not have full connectivity but required some travel time via slower diffusive transport through unconnected matrix grid cells—only diffusive transport is represented in the ECPM grid cells not directly intersected by DFN fractures. The difference in travel time (Fig. 7) is quite apparent between connected realizations and unconnected realizations, showing that the waste isolation safety function for the natural barrier (i.e., the far-field crystalline host-rock domain) can vary in robustness depending on the location of a sited repository relative to the distribution of fractures and deterministic features.

3-D Spatial Profiles of [^{129}I] – Connected vs. Unconnected Fracture Maps

Fig. 8 shows spatial profiles of ^{129}I concentration at three different times (400 yr, 10,000 yr, and 100,000 yr) for a "connected" fracture-map realization versus an "unconnected" realization. At 10,000 years diffusive transport has yet to allow radionuclides to reach a fast fault pathway to the surface for the *unconnected* realization. However, eventually (by 100,000 years) radionuclides have diffused to the fast pathways and then quickly reach the surface, albeit at a relatively low concentration level (only about 10^{-15} mol/L). Similar differences exist between other of the connected and unconnected fracture map realizations—not shown here.

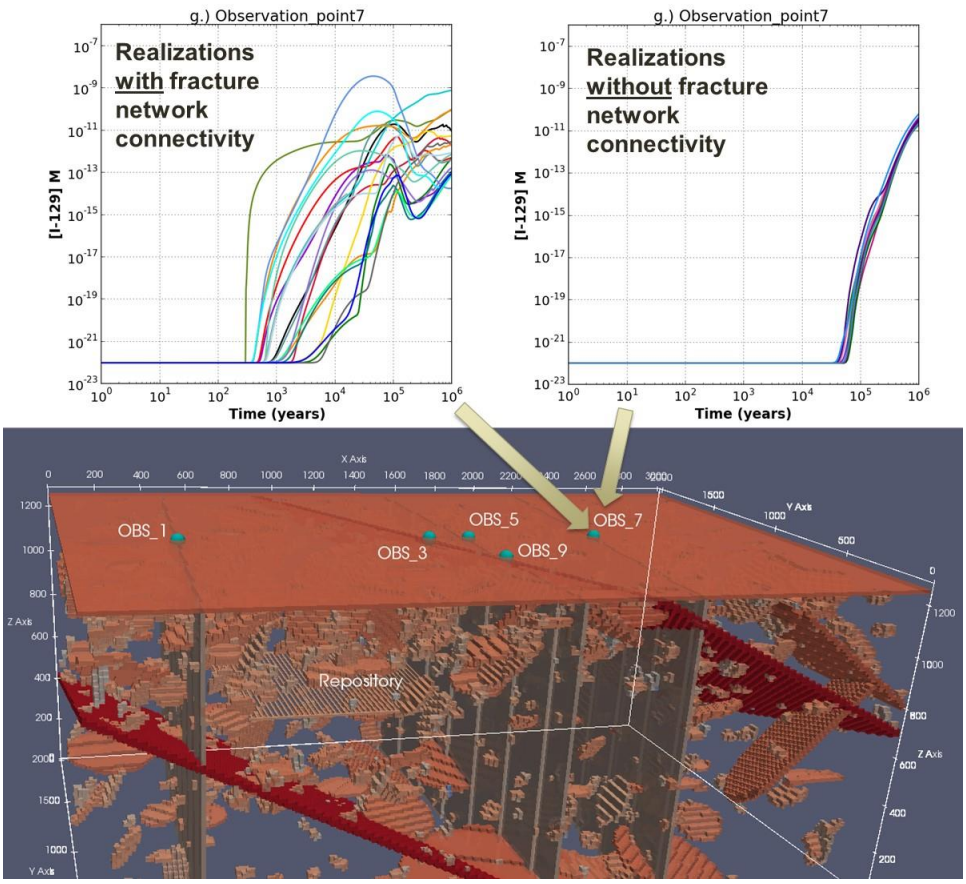

Fig. 7. Comparison of [^{129}I] breakthrough curves (in the upper sedimentary layer) between connected and unconnected fracture-map realizations.

SUMMARY AND CONCLUSIONS

Performance assessment simulations of a generic mined repository in fractured crystalline rock using stochastically generated fracture networks illustrate that radionuclide plume migration depends on the location and density of randomly distributed fractures relative to fixed deformation and fault zones. The key safety concern is the potential effect on waste isolation of the inter-connectivity of the fracture network, which is primarily established by the temporal evolution of the temperature and stress fields at the time of original rock intrusion and cooling. Two end members are considered in this study, one with a high degree of connectivity to the biosphere, such that advective transport through the fracture and fault network controls radionuclide migration, and the other with a low degree of connectivity, such that slow diffusive transport through the crystalline rock matrix is the controlling process for migration to the biosphere. Both end members have several areally extensive, high-transmissivity deformation zones. Uncertainties in fracture properties (transmissivity, orientation, radius) and fracture distribution give rise to uncertainty in waste isolation capability (i.e., the overall connectivity of the repository with the surface biosphere), depending on the distance of the repository to the nearest deformation zone. These types of natural system uncertainties are generally present in any geologic site-characterization program and thus represent an important factor in assessing repository performance in hard rock environments.

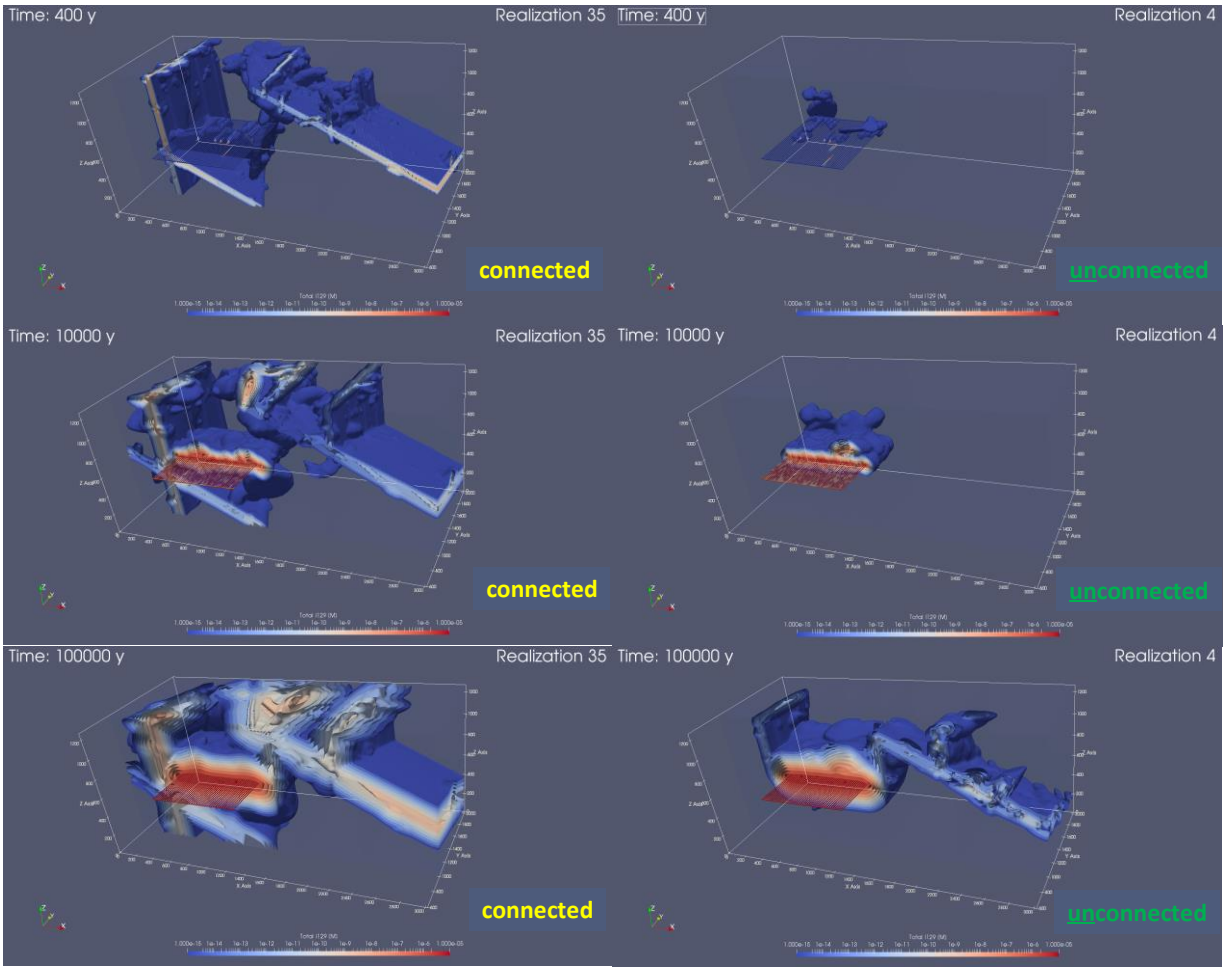

Fig. 8. Comparison of [^{129}I] spatial profiles at various times (400 yr, 10,000 yr, 100,000 yr) for a connected versus an unconnected fracture-map realization.

The waste considered in these simulations are spent fuel rod assemblies from the U.S. commercial nuclear reactor fleet. To achieve a high-fidelity representation of radionuclide transport in fractures and rock matrix, combined with thermal energy transport and fluid flow in fractures and matrix, the mathematical model is solved numerically in a parallel high-performance computing (HPC) environment on a finite volume unstructured grid consisting of approximately 5 million cells, using *Geologic Disposal Safety Assessment* (*GDSA*) *Framework* (https://pa.sandia.gov), an open-source performance assessment tool for deep underground disposal of nuclear waste. *GDSA Framework* uses PFLOTRAN to solve the balance equations on a three-dimensional grid with heterogeneous properties, using multiple processors in a parallel configuration, achieved with PETSc libraries. The fracture networks in these simulations are originally generated as discrete fracture networks (DFNs), which are sets of two-dimensional planes distributed in a three-dimensional domain. The method used in *GDSA Framework* maps the stochastically generated DFN to an equivalent continuous porous medium (ECPM) domain that allows for the simulation of coupled heat flow, fluid flow, and radionuclide transport, including heat conduction through the matrix of the fractured rock, which is a process not easily modeled in a DFN representation. Computational efficiency is also greatly enhanced using the ECPM method, allowing for a realistic representation and analysis of uncertainties in a multi-realization performance assessment of a deep geologic repository.

The effect of fracture connectivity on the waste isolation safety function as brought to light by these *GDSA Framework* simulations points to the importance of including a realistic representation of uncertainties in fracture properties and distribution (effectively, uncertainty in spatial heterogeneity) in repository safety assessment simulations.

REFERENCES

1. Sevougian, S. D., G. A. Freeze, W. P. Gardner, G. E. Hammond, P. Mariner, and R. J. MacKinnon. 2015. "Performance Assessment Modeling of a Generic SNF/HLW Repository in Salt with Coupled Thermal-Hydrologic Effects – 15423," in *Proceedings of the WM2015 Conference*, March 15 – 19, 2015, Phoenix, Arizona USA.
2. Sevougian, S. D., E. R. Stein, G. E. Hammond, P. E. Mariner, and W. P. Gardner 2016. "Enhanced Performance Assessment Models for Generic Deep Geologic Repositories for High-Level Waste and Spent Nuclear Fuel – 16223," in *Proceedings of the WM2016 Conference*, March 6 – 10, 2016, Phoenix, Arizona USA.
3. Adams, B.M., M.S. Ebeida, M.S. Eldred, J.D. Jakeman, K.A. Maupin, J.A. Monschke, L.P. Swiler, J.A. Stephens, D.M. Vigil, T.M. Wildey, W.J. Bohnhoff, K.R. Dalbey, J.P. Eddy, R.W. Hooper, K.T. Hu, P.D. Hough, E.M. Ridgway, A. Rushdi 2016. *Dakota, a Multilevel Parallel Object-Oriented Framework for Design Optimization, Parameter Estimation, Uncertainty Quantification, and Sensitivity Analysis: Version 6.4 User's Manual.* SAND2014-4633, July 2014, Updated May 9, 2016. Sandia National Laboratories, Albuquerque, NM. (http://dakota.sandia.gov/)
4. Hammond, G.E., P.C. Lichtner and R.T. Mills 2014. "Evaluating the Performance of Parallel Subsurface Simulators: An Illustrative Example with PFLOTRAN", *Water Resources Research*, 50, doi:10.1002/2012WR013483.
5. Lichtner, P. C., G. E. Hammond, C. Lu, S. Karra, G. Bisht, B. Andre, R. Mills, and J. Kumar 2015. *PFLOTRAN User Manual: A Massively Parallel Reactive Flow and Transport Model for Describing Surface and Subsurface Processes*, http://www.pflotran.org/docs/user_manual.pdf, January 20, 2015
6. SKB (Svensk Kärnbränslehantering AB) 2007. *Geology Forsmark*. R-07-45 Swedish Nuclear Fuel and Waste Management Co., Stockholm, Sweden.
7. Mariner, P., J. H. Lee, E. Hardin, F. D. Hansen, G. Freeze, A. S. Lord, B. Goldstein, and R. H. Price 2011. *Granite Disposal of U.S. High-Level Radioactive Waste*. SAND2011-6203. Sandia National Laboratories, Albuquerque, NM.
8. Freeze, G., M. Voegele, P. Vaughn, J. Prouty, W.M. Nutt, E. Hardin, and S.D. Sevougian 2013. *Generic Deep Geologic Disposal Safety Case*. FCRD-UFD-2012-000146 Rev. 1, SAND2013-0974P, August 2013, Sandia National Laboratories, Albuquerque, NM.
9. SKB (Svensk Kärnbränslehantering AB) 2011. *Long-term safety for the final repository for spent nuclear fuel at Forsmark: Main report of the SR-Site project* (3 volumes). TR-11-01. Swedish Nuclear Fuel and Waste Management Co., Stockholm, Sweden. (www.skb.se/publications)
10. Mariner, P. E., E. R. Stein, J. M. Frederick, S. D. Sevougian, G. E. Hammond, and D. G. Fascitelli 2016. *Advances in Geologic Disposal System Modeling and Application to Crystalline Rock*, FCRD-UFD-2016-000440, SAND2016-96107R. Sandia National Laboratories, Albuquerque, NM, September 22, 2016.
11. Follin, S., L. Hartley, I. Rhen, P. Jackson, S. Joyce, D. Roberts, and B. Swift 2014. "A methodology to constrain the parameters of a hydrogeological discrete fracture network model for sparsely fractured crystalline rock, exemplified by data from the proposed high-level nuclear waste repository site at Forsmark, Sweden," *Hydrogeology Journal, 22*(2), 313-331. doi: 10.1007/s10040-013-1080-2
12. Joyce, S., L. Hartley, D. Applegate, J. Hoek, and P. Jackson 2014. "Multi-scale groundwater flow modeling during temperate climate conditions for the safety assessment of the proposed high-level nuclear waste repository site at Forsmark, Sweden". *Hydrogeology Journal, 22*(6), 1233-1249.
13. SKB (Svensk Kärnbränslehantering AB) 2007. *Geology Forsmark*. R-07-45 Swedish Nuclear Fuel and Waste Management Co., Stockholm, Sweden.
14. Perry, F. V., R. E. Kelley, and D. M. Milazzo 2016. *Regional Geologic Evaluations for Disposal of HLW and SNF: Archean Crystalline Rocks of the North-Central United States*. FCRD-UFD-2016-000634; LA-UR-16-27845. Los Alamos National Laboratory, Los Alamos, NM.
15. Wang, Y., et al. 2014. *Used Fuel Disposal in Crystalline Rocks: Status and FY14 Progress*, FCRD-UFD-2014-000060, SAND2014-17992R, Sandia National Laboratories, Albuquerque, New Mexico, September 2014.
16. Schild, M., S. Siegesmund, A. Vollbrecht, and M. Mazurek 2001. "Characterization of granite matrix porosity

and pore-space geometry by in situ and laboratory methods". *Geophysical Journal International, 146*(1), 111-125. doi: 10.1046/j.0956-540x.2001.01427.x
17. Soler, J. M., J. Landa, V. Havlova, Y. Tachi, T. Ebina, P. Sardini, M. Siitari-Kauppi, J. Eikenberg, and A. J. Martin 2015. "Comparative modeling of an in situ diffusion experiment in granite at the Grimsel Test Site". *Journal of Contaminant Hydrology, 179*, 89-101. doi: 10.1016/j.jconhyd.2015.06.002
18. Martino, J. B. and N. A. Chandler 2004. "Excavation-induced damage studies at the Underground Research Laboratory". *International Journal of Rock Mechanics and Mining Sciences, 41*(8), 1413-1426.
19. Cho, W.-J., J.-S. Kim, C. Lee, and H.-J. Choi 2013. "Gas permeability in the excavation damaged zone at KURT". *Engineering Geology, 164*, 222-229. doi: 10.1016/j.enggeo.2013.07.010
20. Carter, J. T., A. J. Luptak, J. Gastelum, C. Stockman, and A. Miller 2013. *Fuel Cycle Potential Waste Inventory for Disposition*. FCRD-USED-2010-000031 Rev 6. Savannah River National Laboratory, Aiken, SC.
21. Freeze, G., W. P. Gardner, P. Vaughn, S. D. Sevougian, P. Mariner, V. Mousseau and G. Hammond 2013. *Enhancements to the Generic Disposal System Modeling Capabilities*. SAND2013-10532P. Sandia National Laboratories, Albuquerque, New Mexico.
22. Shelton, S. M. 1934. "Thermal conductivity of some irons and steels over the temperature range 100 to 500 C," *Bureau of Standards Journal of Research*, **12**(4/6):441-450.
23. Frederick, J. M., G. E. Hammond, P. E. Mariner, E. R. Stein and S. D. Sevougian 2017. "Development of a Waste Form Process Model in PFLOTRAN." *Proceedings of the International High-Level Radioactive Waste Management Conference, Charlotte, NC, April 9-13, 2017*.
24. Choi, H. J. and J. Choi (2008). "Double-layered buffer to enhance the thermal performance in a high-level radioactive waste disposal system," *Nuclear Engineering and Design*, **238**(10):2815-2820.
25. Jobmann, M. and G. Buntebarth (2009). "Influence of graphite and quartz addition on the thermo-physical properties of bentonite for sealing heat-generating radioactive waste," *Applied Clay Science*, **44**(3-4):206-210.
26. Wang, M., Y. F. Chen, S. Zhou, R. Hu, and C. B. Zhou 2015. "A homogenization-based model for the effective thermal conductivity of bentonite-sand-based buffer material". *International Communications in Heat and Mass Transfer*, **68**:43-49.
27. Liu, J. F., Y. Song, F. Skoczylas and J. Liu (2016). "Gas migration through water-saturated bentonite-sand mixtures, CO_x argillite, and their interfaces," *Canadian Geotechnical Journal*, **53**(1):60-71.
28. Sassani, D. C., C. F. Jové Colón, P. Weck, J. L. Jerden, K. E. Frey, T. Cruse, W. L. Ebert, E. C. Buck, R. S. Wittman, F. N. Skomurski, K. J. Cantrell, B. K. McNamara and Z. Soderquist (2012). *Integration of EBS Models with Generic Disposal System Models*. SAND2012-7762P. Sandia National Laboratories, Albuquerque, New Mexico.
29. Sassani, D., J. Jang, P. Mariner, L. Price, R. Rechard, M. Rigali, R. Rogers, E. Stein, W. Walkow and P. Weck (2016). *The On-line Waste Library (OWL): Usage and Inventory Status Report*. FCRD-UFD-2016-000080. Sandia National Laboratories, Albuquerque, New Mexico.
30. Freeze, R. A. and J. A. Cherry (1979). *Groundwater*. Englewood Cliffs, New Jersey, Prentice-Hall, Inc.
31. Mariner, P. E., W. P. Gardner, G. E. Hammond, S. D. Sevougian, and E. R. Stein 2015. *Application of Generic Disposal System Models*. SAND2015-10037R; FCRD-UFD-2015-000126. Sandia National Laboratories, Albuquerque, NM.
32. Balay S., J. Brown, K. Buschelman, V. Eijkhout, W.D. Gropp, D. Kaushik, M.G. Knepley, L. Curfman McInnes, B.F. Smith and H. Zhang 2013. *PETSc Users Manual*, ANL-95/11 – Revision 3.4, Argonne National Laboratory, Argonne IL.
33. Blacker, T., S. J. Owen, M. L. Staten, R. W. Quador, B. Hanks, B. Clark, R. J. Meyers, C. Ernst, K. Merkley, R. Morris, C. McBride, C. Stimpson, M. Plooster, and S. Showman 2016. *CUBIT Geometry and Mesh Generation Toolkit 15.2 User Documentation*. Sandia National Laboratories, Albuquerque, NM.
34. Li, Y. H. and S. Gregory 1974. "Diffusion of Ions in Sea-Water and in Deep-Sea Sediments," *Geochimica Et Cosmochimica Acta*, *38*(5), 703-714.
35. Hyman, J. D., S. L. Painter, H. Viswanathan, N. Makedonska, and S. Karra 2015. "Influence of injection mode on transport properties in kilometer-scale three-dimensional discrete fracture networks," *Water Resources Research, 51*(9), 7289-7308. doi: 10.1002/2015wr017151
36. Hyman, J. D., S. Karra, N. Makedonska, C. W. Gable, S. L. Painter, and H. S. Viswanathan 2015. "dfnWorks: A discrete fracture network framework for modeling subsurface flow and transport," *Computers & Geosciences, 84*, 10-19. doi: 10.1016/j.cageo.2015.08.001
37. Bear, J., C. F. Tsang, and G. de Marsily 1993. *Flow and Contaminant Transport in Fractured Rock*, San Diego, CA: Academic Press, Inc.

38. Stein, E. R., J. M. Frederick, G. E. Hammond, K. L. Kuhlman, P. E. Mariner, and S. D. Sevougian 2017. "Modeling Coupled Reactive Flow Processes in Fractured Crystalline Rock," in *Proceedings of the International High-Level Radioactive Waste Management (IHLRWM 2017) Conference*, April 9 – 13, 2017, Charlotte, NC.
39. Parashar, R., and D. M. Reeves (2011). *Computation of flow and transport in fracture networks on a continuum grid*. In: Proceedings of MODFLOW and MORE 2011: Integrated Hydrologic Modeling, Golden, CO. 5–8 June 2011. Int. Ground Water Model. Ctr., Colorado School of Mines, Golden. p. 752–756.

ACKNOWLEDGEMENTS

The authors would like to thank Frank Perry (LANL), who gave important insights regarding potential crystalline host rock formations in the U.S., as well as members of the LANL dfnWorks Team, who helped with fracture mapping and representation of the natural system, including Hari Viswanathan (LANL), Satish Karra (LANL), Jeffrey Hyman (LANL), and Nataliia Makedonska (LANL). Ernie Hardin (SNL) provided detailed knowledge regarding repository design and thermal constraints. Sandia National Laboratories is a multi-mission laboratory managed and operated by National Technology and Engineering Solutions of Sandia LLC, a wholly owned subsidiary of Honeywell International Inc. for the U.S. Department of Energy's National Nuclear Security Administration under contract DE-NA0003525. This paper is Sandia publication SAND2017-XXXXX C.